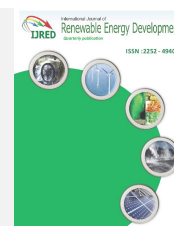




Contents list available at IJRED website

Int. Journal of Renewable Energy Development (IJRED)

Journal homepage: <http://ejournal.undip.ac.id/index.php/ijred>



Research Article

Two-Phase Expander Approach for Next Generation of Heat Recovery Systems

Angad S. Panesar* and Marco Bernagozzi

Advanced Engineering Centre, School of Computing, Engineering and Mathematics, University of Brighton, United Kingdom

ABSTRACT. This study presents the numerical adaptations to the semi-empirical expander model in order to examine the feasibility of piston expanders under off-design and two-phase scenarios. This expander model considers supply valve pressure drop, condensation phenomena, heat losses, leakage losses and friction losses. Using Aspen HYSYS[®], the expander model is utilised in simulating the next generation of integrated engine cooling and exhaust heat recovery system for future heavy-duty engines. The heat recovery system utilises water-propanol working fluid mixture and consists of independent high pressure (HP) and low pressure (LP) expander. The results of off-design and two-phase operation are presented in terms of expander efficiency and the different sources of loss, under two distinctive engine speed-load conditions. The heat recovery system, operating with the LP expander at two-phase and the HP expander at superheated condition, represented the design point condition. At the design point, the system provided 15.9 kW of net power, with an overall conversion efficiency of 11.4%, representing 10% of additional engine crankshaft power. At the extreme off-design condition, the two-phase expander operation improved the system performance as a result of the nullification of leakage losses due to the much denser working fluid. The optimised two-phase operation of the LP expander ($x=0.55$) and the HP expander ($x=0.9$) at the extreme-off design condition improved the system power by nearly 50% (17.4 vs. 11.7 kW) compared to the reference state. Finally, adapting piston air motors as two-phase expanders for experimental evaluation and reduction in frictional losses was a recommended research direction. ©2019. CBIORÉ-IJRED. All rights reserved

Keywords: Two-Phase, Waste Heat Recovery, Piston Expander, Friction, Heat Transfer

Article History: Received: Sept 11, 2019; Revised: Oct 20, 2019; Accepted: Oct 25, 2019; Available online: Oct 30, 2019

How to Cite This Article: Panesar, A.S., Bernagozzi, M., (2019) Two-Phase Expander Approach for Next Generation of Heat Recovery Systems. International Journal of Renewable Energy Development, 8(3), 203-213
<https://doi.org/10.14710/ijred.8.3.203-213>

1. Introduction

The efficiency improvements for the heavy-duty combustion engines are being driven by issues such as increasing greenhouse emissions, stringent fuel-consumption regulations and diminishing fossil fuel supplies (*EU Energy Efficiency Plan*, 2011). Research and development efforts are focusing on: new engine architectures (e.g. split cycle), powertrain efficiency enhancements (e.g. waste heat recovery) and sustainable fuels (e.g. biodiesel) (Automotive Council and Advanced Propulsion Centre, 2018). In the haulage sector, the demonstrated versions of thermo-electric generators and Organic Rankine Cycle (ORC) systems on exhaust heat recovery are prospective starting points for improving the overall system efficiency (BorgWarner, 2018).

An influential component in the ORC systems is an efficient and versatile expansion device (Lemort, Declaye, & Quoilin, 2012). They can be either velocity based (e.g. axial turbine, radial turbine), which are preferred for medium kW output and beyond (Saghatoun, Zhuge, & Zhang, 2014); or volume based (e.g. screw expander, piston expander) which are suitable for low to medium kW output (Imran, Usman, Park, & Lee, 2016). By allowing

consideration of a two-phase expansion approach, volumetric expanders additionally allow unique investigations in ORC improvements (Pikra & Rohmah, 2019; Tchanche, Lambrinos, Frangoudakis, & Papadakis, 2011) and moisture control (Kanaš, Jedlikowski, & Anisimov, 2019). These can be either to limit the challenges of ensuring superheat to prevent condensation under dynamic conditions or by improving the overall conversion efficiency under lower grade heat recovery.

The two-phase expansion approach is also appealing in Liquefied Natural Gas (LNG) plants. It has been demonstrated that a preferred option in the liquefaction process of natural gas, which is required for transportation purposes, is introducing a two-phase expansion approach combined with single phase Joule-Thompson (JT) valve (Amsyari et al., 2007). The two-phase expansion exploits the isentropic expansion, instead of the isenthalpic JT valve, providing increased cooling capacity and reducing the energy consumption by nearly 60% compared to the standard N₂ single LNG expander (Qyyum, Qadeer, Lee, & Lee, 2018).

The research on two-phase expanders is additionally motivated by the interest in the trilateral flash cycle for

* Corresponding author: A.S.Panesar@brighton.ac.uk

lower grade heat recovery (Bianchi et al., 2017). Vasuthevan and Brümmer (Vasuthevan & Brümmer, 2016) proposed and experimentally validated the thermodynamic two-phase model of a screw expander where mass and energy balance equations were separated for vapour and liquid states of water. Their major assumption was to consider the thermodynamic equilibrium of the phases during calculation of chamber states, which was identified as the cause of deviations from the experimental data. Bianchi et al. (Bianchi et al., 2017) modelled a twin-screw expander for two-phase operation in the GT-SUITE platform, employing REFPROP for the two-phase properties calculations of R245fa. They achieved the modelling of under/over expansion, as well as leakage losses. However, the two-phase mixture was treated as an equivalent gas and this work excluded the frictional losses.

There are three distinctive approaches for modelling the performance prediction of a volumetric expander, namely deterministic, empirical and semi-empirical (Dumont, Dickes, & Lemort, 2017). However, the semi-empirical model, where a selected number of equations best describe the important parameters of the system, represents a proven compromise between the limitations of validity range of the empirical models and the computational demand of the deterministic models. Lemort et al. (Vincent Lemort, Quoilin, Cuevas, & Lebrun, 2009) initially presented a semi-empirical model of a scroll expander, which was recently extended by Giuffrida (Giuffrida, 2017) for improvements in the modelled mechanical losses for a single-screw expander utilising the Stribeck's theory. A low error of around 2% in the output power was reported when comparing the expander model to the experimental data.

This work presents the numerical adaptations to the above semi-empirical model in order to examine the feasibility of piston expanders under off-design and two-phase scenarios, in an integrated cooling and heat recovery system for future heavy-duty engines. Firstly, the numerical model of the expander is detailed, including the two-phase adaptations in suction valve pressure drop, heat transfer losses and piston frictional losses. Secondly, a next generation of integrated engine cooling and exhaust heat recovery system, first introduced by the authors (Panesar, 2016), is examined under two distinctive engine speed-load conditions. Finally, using Aspen HYSYS®, the effects of the two-phase expansion approach on the performance of the two independent expanders utilised by the system and on the overall system performance are reported.

2. Numerical Model of the Expander

The expander model presented in this section has been adapted following the efforts of Lemort (Vincent Lemort et al., 2009) and Giuffrida (Giuffrida, 2017) for two-phase operation. The model accounts for several sources of power losses; including, suction pressure loss, leakage loss, heat loss and friction loss, using the following initial assumptions:

- Inlet valve is considered as a throttling valve, i.e. isenthalpic transformation;
- Pressure drop at the outlet is zero;

- Leakages are adiabatic;
- Additives to the working fluid are neglected;
- Expander envelope is isothermal.

The chosen numerical methodology for the expander model was the lumped parameter approach, in which the physical and geometrical properties of real sections are assigned to the corresponding nodes through rational assumptions. Hence, the complexity of introducing the real geometry is avoided, allowing to obtain near-accurate results. Such a modelling strategy has already been adopted by the authors in thermal management works for automotive applications (Bernagozzi et al., 2018), where the lumped parameter model was able to replicate experimental data with an accuracy of nearly 99%.

The abovementioned assumptions allow a one-dimensional representation of the expander, as depicted in Fig. 1. The sub-modelling processes are as follows:

- (0-1) pressure drop through the supply valve;
- (1-2) heat transfer lost with the expander envelope at the inlet;
- (2-3) isentropic expansion;
- (3-4) isochoric expansion;
- (4-5) reunion of nominal mass flow rate \dot{m}_{in} with leakages \dot{m}_{leak} ;
- (5-6) heat transfer loss with expander envelope at the outlet.

Therefore, P_{int} is the net power generated whereas, P_{fric} and P_{leak} are the friction and leakage losses, respectively. Hence, such a model provides the advantage of a common framework for all volumetric expanders by applying an appropriate friction model.

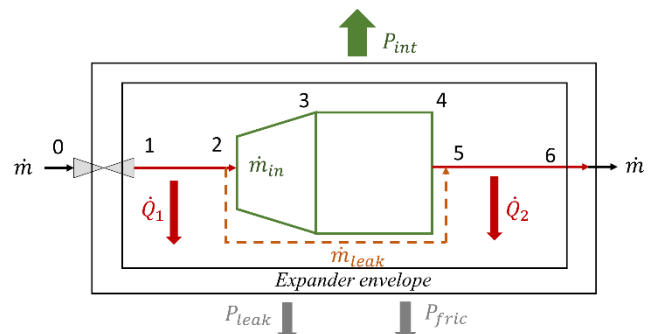


Fig. 1 One-dimensional representation of the expander, showing nodes and losses considered in the numerical model.

The present expander model was coupled with Aspen HYSYS® for calculating at every node the working fluid properties such as, density, specific enthalpy, specific heat at constant pressure, thermal conductivity, viscosity and entropy. Due to the available extensive fluid database and property packages, the earlier identified preferred working fluid for the combined engine cooling and exhaust heat recovery, i.e. water-propanol mixture, was utilised (Panesar, 2017).

The present expander model requires limited input data, which includes:

- Boundary conditions: initial pressure, initial temperature, initial vapour quality, mass flow rate, desired pressure ratio and ambient temperature;
- Expander geometry: inlet radius, diameter,

length, maximum displacement volume, built-in volume ratio and RPM;

- Fluid properties: critical pressure and co-simulation with Aspen HYSYS[®].

2.1 Supply Valve Pressure Drop (0-1)

Aspen HYSYS[®] is an advanced process modelling software which allows the definition of all the thermo-physical properties of a working fluid, once two out of either temperature, pressure or vapour quality are fixed by the user. In the expander model, the starting pressure p_0 , vapour quality x_0 and the mass flow rate \dot{m} are considered to be known, and consequently, all the remaining properties at point 0 are defined.

If the fluid is in a two-phase state at the inlet, i.e. $x < 1$, the vapour and liquid fractions are utilized to calculate the equivalent properties in the two-phase state. An example of a generic two-phase (2p) property ε_{2p} is given below:

$$\varepsilon_{2p} = x\varepsilon_v + (1 - x)\varepsilon_l \quad (1)$$

To calculate the pressure drop at the expander inlet, the isentropic nozzle theory is adopted, considering the vapour properties as:

$$h_{1,is} = h_0 - 0.5 \cdot \left(\frac{\dot{m}}{\rho A_{in}} \right)^2 \quad (2)$$

In case of an isentropic transformation, this gives the entropy at point 1. Which allows identification of pressure $p_1 = f(h_{1,is})$. Therefore, the resulting vapour pressure drop is calculated as:

$$\Delta p_{inlet\ vap} = p_0 - p_1 \quad (3)$$

A thermo-physical fluid property which is directly proportional to the pressure drop through a valve is density. Hence, if the fluid is in a two-phase state at the inlet, then to account for the increased inlet pressure drop, $\Delta p_{inlet\ vap}$ is multiplied by the ratio of the two-phase and vapour densities as:

$$\Delta p_{inlet\ 2p} = \frac{\rho_{2p}}{\rho_v} \Delta p_{inlet\ vap} \quad (4)$$

Since an isenthalpic transformation is considered, i.e. $h_0 = h_1$, the remaining properties at node 1 are fully defined.

2.2. Heat Transfer with Expander Envelope (1-2)

To calculate the heat loss from the working fluid to the envelope wall of the expander, the equation for convection heat transfer is used as:

$$Q = h_c A (T_1 - T_w) \quad (5)$$

If the fluid is in two-phase state, the Shah correlation (Shah, 2009) for heat transfer coefficient is used. Since, compared to other published correlations, it has a lower average prediction error of 20% (Derby, Lee, Peles, & Jensen, 2012) as:

$$h_c = \alpha_f \left[(1 - x)^{0.8} + \frac{3.8x^{0.76}(1 - x)^{0.04}}{p^{*0.38}} \right] \quad (6)$$

where p^* is the reduced pressure, i.e. actual pressure divided by the critical pressure p_c , and α_f is the liquid convection coefficient from Dittus-Boelter (Sánta, 2012) as:

$$\alpha_f = 0.023 Re^{0.8} Pr^{0.3} \frac{k_l}{2r_i} \quad (7)$$

$$p^* = \frac{p_1}{p_c} \quad (8)$$

where k_l is thermal conductivity of the liquid fraction, r_i is the internal radius.

The pressure at point 2 is calculated using the distributed losses formula (Idel'chik, 1960) as:

$$p_2 = p_1 - \dot{m} R_{dist} \quad (9)$$

$$R_{dist} = \frac{8\mu L}{\rho \pi r_{in}^4} \quad (10)$$

where R_{dist} is the distribute hydraulic resistance, μ is kinematic viscosity, L is the length of the considered part of the expander and ρ is the density.

When utilising pure working fluids and azeotropic mixtures, temperature is considered constant during the phase change process. Therefore, by knowing the heat loss at this point, the new specific enthalpy, and hence, the vapour quality is extracted as:

$$h_{new} = h_1 - \frac{Q}{\dot{m}} \quad (11)$$

$$x_{new} = \frac{h_{new} - h_l}{h_v - h_l} \quad (12)$$

As a result, the two-phase state equivalent of all the fluid properties is calculated, and hence, the node 2 is fully defined.

2.3. Isentropic Expansion (2-3)

There is a defined mass flow rate (\dot{m}_{in}) that an expander can host, which is a function of the fluid properties, the geometrical design and the operating condition. Therefore, the excess mass flow (\dot{m}_{leak}), due to off-design operation is considered to be leakages as:

$$\dot{m}_{in} = \frac{\rho_2 N V_{sw}}{BVR} \quad (13)$$

$$\dot{m}_{leak} = \dot{m} - \dot{m}_{in} \quad (14)$$

where N is the RPM, V_{sw} is the maximum displacement volume and BVR is the built-in volume ratio, which is defined as the volume of the expansion chamber at the end of the expansion process over the volume of the expansion chamber at the beginning of the expansion process (Oralli, Tarique, Zamfirescu, & Dincer, 2011).

Assuming isentropic expansion, it is possible to deduce point 3 values as:

$$s_{3,2p} = s_{2,2p} \quad (15)$$

$$v_3 = BVR \cdot v_2 \quad (16)$$

Therefore, utilising the above two values in Aspen HYSYS[®], it is possible to identify the pressure and vapour quality, and hence, the node 3 is fully defined.

2.4. Isochoric Expansion (3-4)

The outlet pressure (P_4) is governed by the expander pressure ratio (PR). Therefore, considering an isochoric expansion leads to identification of point 4 values as:

$$p_4 = \frac{p_0}{PR} \quad (17)$$

$$v_{4,2p} = v_{3,2p} \quad (18)$$

Utilising the above two values in Aspen HYSYS[®], it is possible to identify the single-phase properties as well as the vapour fraction, and hence, the node 4 is fully defined. Furthermore, point 4 gives an indication on the level of under/over expansion due to the equation describing the off-design expansion process as (Giuffrida, 2017):

$$h_{4,2p} = h_{3,2p} - v_{3,2p}(p_3 - p_4) \quad (19)$$

During under-expansion, the pressure at the end of the isentropic processes is higher than the expander outlet, vice versa occurs during over-expansion.

2.5. Mass Flow Rate Reunion (4-5)

Point 5 accounts for the reunion of the mass flow rate from the expansion process at point 4 and leakage process at point 2. This results in the change in specific enthalpy as:

$$h_5 = \frac{h_{4,2p}\dot{m}_4 + h_{2,2p}\dot{m}_{leak}}{(\dot{m}_4 + \dot{m}_{leak})} \quad (20)$$

Utilising the above value in Aspen HYSYS[®], it is possible to identify the vapour fraction, and hence, the node 5 is fully defined.

2.6 Heat Transfer with Expander Envelope (5-6)

The total working fluid mass flow rate exchanges heat loss again with the envelope. Assuming no change in the temperature for pure working fluids and azeotropic mixtures during the phase change process, the heat transfer calculation is carried out using the same procedure detailed in section 2.2. This allows the node 6 to be fully defined.

2.7 Expander Efficiency and Power

Fig. 2 illustrates the overall real expansion process in the model (solid black line) and compares it to an ideal isentropic expansion (dashed grey line) when the enthalpy value of the fluid ($h_{6,is}$) brought down to the pressure maintained by the condenser (p_6).

In this analysis, the net expander work (P_{int}), is produced by the expander taking only the mass flow rate hosted during the expansion (i.e. node 2-4), and is calculated as:

$$P_{int} = \dot{m}_{int}(h_2 - h_4) - P_{fric} - P_{heat} \quad (21)$$

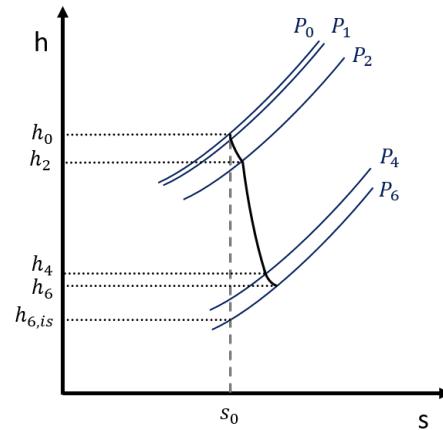


Fig. 2 Representation of the change in enthalpy, entropy and pressure in the overall generic real expansion process modelled against the ideal isentropic expansion.

where P_{heat} is the cumulative power loss due to heat transfer, calculated as the sum of the heat losses between 1-2 and 5-6. Since the piston expander was considered in the present work, a modified Chenn-Flynn model (Chen & Flynn, 1965) is used to estimate the frictional losses. According to this model, the Friction Mean Effective Pressure (FMEP) is a function of the in-cylinder maximum pressure P_2 and a speed factor S_f .

$$FMEP = A + B \cdot P_{max} + C \cdot S_f + D \cdot S_f^2 \quad (22)$$

where invariable factors include, A (0.9 bar) which accounts for the auxiliary losses, B (0.018) which accounts for the in-cylinder pressure, and C (0.15 bar·s/m) and D (0.000255 bar·s²/m) which accounts for rotational speed. The above considered constants are representative of comparable scale of automotive piston engines. The speed factor is calculated using the piston stroke (S) as:

$$S_f = \frac{\pi NS}{60} \quad (23)$$

The FMEP is translated into power loss as:

$$P_{fricCF} = \frac{FMEP \cdot V_{sw} \cdot N}{2} \quad (24)$$

A thermo-physical fluid property which is directly proportional to friction power is viscosity. Hence, if the fluid is in a two-phase state, in order to account for the increased friction power, P_{fricCF} is multiplied by the ratio of the two-phase and vapour viscosities as:

$$P_{fricCF,2p} = \frac{\mu_{2p}}{\mu_v} \cdot P_{fricCF} \quad (25)$$

Therefore, the accurate overall real isentropic efficiency for the expander is defined as:

$$\eta = \frac{P_{int}}{\dot{m}(h_0 - h_{6,is})} \quad (26)$$

3. Next Generation of Heat Recovery System for Heavy-Duty Engines

This section presents the new research and development direction for the next generation of heat recovery systems applied to heavy-duty combustion engines, in particularly, long-haul Diesel vehicles. An integrated engine cooling and exhaust heat recovery system (Fig. 3), which was first proposed by the authors (Panesar, 2017), is considered using two-phase and superheated expansion approach. This integrated system uses a single working fluid to recover heat directly from the engine block and the exhaust heat exchanger by utilising a dual pressure architecture. In Fig. 3, the pumps (low pressure LP, high pressure HP) are responsible for generating the different optimal sub-system pressure levels. Power is produced using two mechanically independent versatile piston expanders (low pressure LP, high pressure HP). A water blend screening study involving over 500 working fluid candidates indicated, the azeotropic water-alcohol blend as 27% water and 73% 1-propanol by mass (hereafter referred to as W28), as the preferred solution. The key thermo-physical properties of the blend and its pure constituents at 100°C liquid are given in Table 1 Compared to a conventional cascade system, it has been shown that this integrated system with conventional expansion has the potential to deliver an average of 20% improvement in the system power and a 50% reduction in the total heat exchanger footprint (Panesar, 2017).

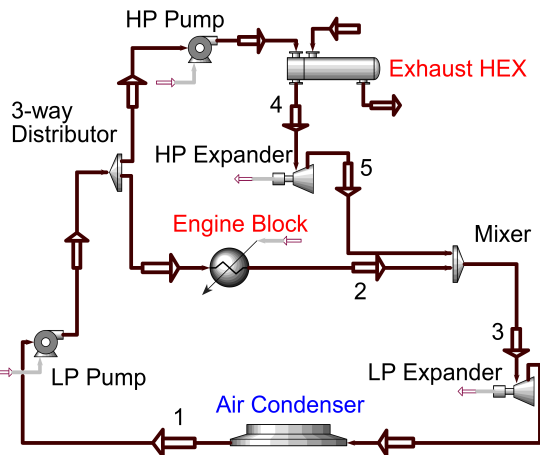


Fig. 3 Schematic of the dual pressure level system for integrated engine cooling and exhaust heat recovery using two phase and superheated expansion approach (Panesar, 2017).

Table 1

Water, propanol and W28 fluid properties at 100°C saturated liquid condition for comparison.

	Mol Weight [g/mol]	ρ [kg/m ³]	c_p [J/kg·K]	h_{LV} [J/kg]	λ [W/m·K]	μ [Pa·s]
Water	18	709	4198	$2.3 \cdot 10^6$	3.53	$1.3 \cdot 10^{-4}$
Propanol	60.1	634	3308	$6.9 \cdot 10^5$	0.29	$4.7 \cdot 10^{-4}$
W28	36.9	651	3736	$1.1 \cdot 10^6$	0.89	$2.3 \cdot 10^{-4}$

The above heat recovery system was coupled with a validated 10L Euro-6 Diesel engine model. Two distinctive engine speed-load conditions were considered, a typical cruise condition (B50) as the design point, and the high-speed high-load condition (C100) as the extreme off-

design point. Table 2 summarises firstly, the engine parameters; secondly, the exhaust heat exchanger or the high-pressure loop parameters; thirdly, the engine block or the low pressure loop parameters; and finally, the engine radiator or the air condenser parameters utilised.

To estimate the varied heat recovery and heat rejection thermal loads during the design point and the off-design point conditions, the overall heat transfer coefficient (U , W/m²C) multiplied by the heat transfer area (A , m²) for the exhaust heat exchanger (1000 W/°C) and the air condenser (5000 W/°C) were kept fixed. The size of the heat transfer equipment's was modelled such that, the existing cooling margin available in the engine cooling module from 6.35 kg/s of air flow was fully utilised at B50, without any additional fan power consumption.

Table 2.

Combustion engine, exhaust heat exchanger/high pressure loop, engine block/low pressure loop and engine radiator/air condenser parameters for the coupled engine and heat recovery analysis.

Variable	Value
Engine parameters (B50 / C100)	
$\eta_{brake\ thermal}$	42.9 / 41.4%
$\dot{W}_{crankshaft}$	158 / 316 kW
Speed	1440 / 1720 rpm
Exhaust heat exchanger or HP loop parameters	
$T_{exhaust\ max}$	423 / 493 °C
$\dot{m}_{exhaust}$	0.212 / 0.408 kg/s
$c_{p\ exhaust}$	1.15 kJ/kg°C
$\Delta P_{EXH\ HEX}$	0.25 bar
$UA_{EXH\ HEX}$	1000 W/°C
$T_{EXH\ pinch\ point}$	40 °C
$T_{max\ HP}$	250 °C
$T_{evaporation\ HP}$	202 °C
$PR_{expander\ HP}$	10:1
Engine block or LP parameters	
$\dot{Q}_{engine\ block}$	69 / 139 kW
$\Delta P_{engine\ block}$	0.25 bar
$T_{evaporation\ LP}$	113 °C
$PR_{expander\ LP}$	4.4:1
Engine radiator or air condenser parameters	
$T_{cooling\ air\ inlet}$	30 °C
$T_{cooling\ air\ exit}$	50 °C
$\eta_{fan\ cond.}$	65%
$\Delta P_{fan\ cond.}$	250 Pa
$\Delta P_{cond.}$	0.25 bar
$UA_{cond.}$	5000 W/°C
$T_{cond.\ pinch\ point}$	30 °C
$\dot{m}_{cooling\ module}$	6.35 kg/s
$\eta_{pump\ LP,\ HP}$	55%

4. Results and Discussion: Expander and System Level Model

This section presents the results of the two studies, in which the HP expander designed for a superheated state (50°C superheat) and the LP expander designed for a two-phase state (0.75 vapour quality) were considered for

off-design operation. Firstly, by fixing the design point BVR, and secondly, by utilising the inlet fluid conditions, the two expander efficiencies were optimised by varying the inlet and the displacement geometrical dimensions. Table 3 summarises the design point fluid and geometrical parameters for the two piston expanders, using the B50 engine condition for heat recovery. Additionally, the expanders were considered geared 1:1 to the engine crankshaft.

Table 3.

Key design point parameters for the high pressure vapour and the low pressure two-phase expander.

	HP Expander	LP Expander
Inlet fluid condition	50°C superheat 23.8 bar (fixed) 0.1 kg/s	0.75 vapour quality 2.6 bar (fixed) 0.3 kg/s
Pressure Ratio	10:1	4.5:1
Built-in Volume Ratio	8:1	8:1
Inlet radius	0.005 m	0.01 m
Maximum displacement volume (Bore Stroke)	0.0007 m ³	0.00027 m ³
Ambient temperature	25 °C	25 °C
Expander efficiency	86%	62%
Expander power	9.1 kW	7.3 kW

Table 4

Evolution of temperature, pressure and vapour quality for the high pressure vapour and the low pressure two-phase expander at the design point condition.

Node	HP Expander (T[°C] / P[bar] / x)	LP Expander (T[°C] / P[bar] / x)
0	250 / 23.5 / superheated	112.7 / 2.35 / 0.75
1	250 / 23.42 / superheated	112.3 / 2.33 / 0.75
2	249.9 / 23.41 / superheated	112.3 / 2.32 / 0.73
3	117.2 / 2.4 / superheated	57 / 0.25 / 0.73
4	117 / 2.35 / superheated	73.2 / 0.53 / 0.7
5	117 / 2.35 / superheated	73.3 / 0.53 / 0.7
6	116.9 / 2.34 / superheated	73.2 / 0.53 / 0.69

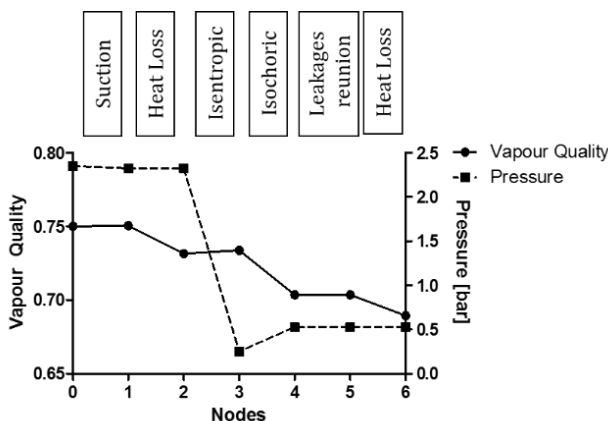


Fig. 4 Vapour quality and pressure evolution inside the two-phase low pressure expander nodes at the design point condition.

The model described in Section 2 allows the tracking of the thermo-physical properties along the different nodes in the overall expansion processes, including temperature, pressure and vapour quality. For the two piston expanders, the design point values at the different nodes are presented in Table 4. Additionally, Fig. 4 shows the evolution of vapour quality and pressure for the LP two-phase expander nodes. A key contributor to the limited design point efficiency of the LP vs. the HP expander in Table 3 (62 vs. 86%) is due to the noticeable thermal losses shown in Fig. 4 (Node 1-2 and 5-6), as a result of the increased heat transfer for two-phase flow.

Two studies were conducted at the B50 and C100 engine heat recovery conditions following the optimisation of the design point expanders:

- Study 1 - Reducing the HP expander inlet vapour quality from superheated state to 0.8, while maintaining the near design point operation of the LP expander.
- Study 2 - Varying the LP expander inlet vapour quality from 0.95 to 0.45, while maintaining the design point operation of the HP expander.

The following sub-sections present the findings of these studies.

4.1 Study 1 - Off-design Operation of the HP Expander

Presentation and discussion of the results are divided into the main parameters of interest, namely, expander isentropic efficiency and losses (i.e. heat, friction and leakages). In Fig. 5, it can be noticed that, at the design-point B50 engine condition, the HP expander efficiency decreases significantly (Fig. 5a) with the reduction in the vapour quality, due to increased heat transfer (Fig. 5b) and frictional losses (Fig. 5c). However, at the extreme off-design C100 engine condition, the HP expander offers an interesting opportunity. As expected, initially superheated HP expansion at C100 presents a lower efficiency compared to B50, due to the increased leakage losses (Fig. 5d) as a result of higher mass flow rate (0.06 kg/s vs 0.13 kg/s). Nonetheless, with the reduction in the vapour fraction to 0.9, an HP expansion efficiency peak is observed. This counter intuitive result is due to the nullification of the leakage losses (Fig. 5d), due to greater mass flow rate being admitted into the expander as a result of the two-phase fluid being denser. Hence, the HP expander offers improvement in efficiency (58% vs. 48%) when operated with a vapour fraction of 0.9 at C100 compared to the reference superheated inlet state. Reducing the vapour fraction beyond 0.8 negates the efficiency gains due to increasing heat transfer and frictional losses.

The heat transfer loss (Fig. 5b) in the HP expander increase with the reduction in the vapour quality due to the increasing convective heat transfer coefficient. At the C100 off-design condition, heat transfer losses are more pronounced due to the higher mass flow rate (increased fluid velocity), and therefore higher convective heat transfer coefficient. Moreover, the C100 higher mass flow rate is also the reason why the slopes of the two HP cases are diverging below a vapour quality of 0.9

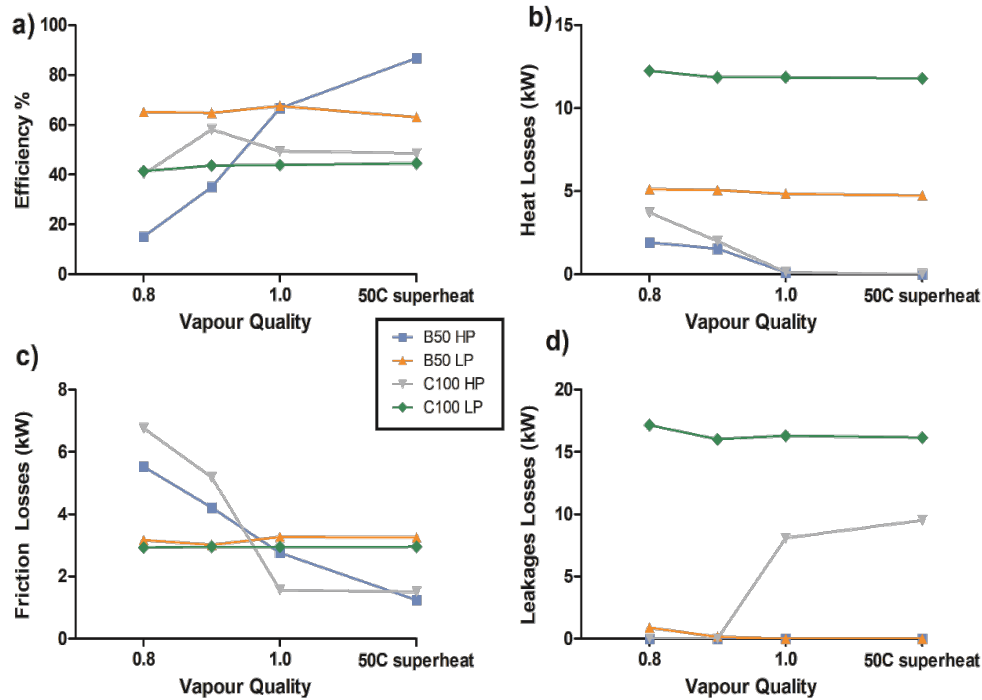


Fig. 5. Study 1: a) expander efficiency, b) heat losses, c) friction losses and d) leakage losses, when HP inlet vapour quality was reduced, whereas LP inlet vapour quality was fixed at 0.75.

Table 5.

Integrated engine cooling and exhaust heat recovery results at the B50 design-point, C100 extreme off design point with non-optimal and C100 extreme off design point with optimal HP expander inlet vapour quality. All with fixed LP vapour quality.

Study 1	Units	B50	C100	C100
		HP	HP	HP
		Expander	Expander	Expander
		50°C	50°C	x=0.9,
		Superheat	Superheat	Optimal
		Design-point	Non-optimal	off-design
			off-design	
$P_{system\ min}$	bar	0.3	1	1
$T_{system\ min}$	°C	59	89	89
$VFR_{expander}(HP)$		8.6:1	9.6:1	9.9:1
$\dot{W}_{expander}(HP)$	kW	9	10.6	12.2
$\dot{W}_{pump}(HP)$	kW	0.3	0.6	0.7
$\dot{m}_{fluid}(HP)$	kg/s	0.047	0.1	0.12
$T_{condensation}(LP)$	°C	66	93	93
$VFR_{expander}(LP)$		4.2:1	1.8:1	1.8:1
$\dot{W}_{expander}(LP)$	kW	7.3	4.9	4.8
$\dot{W}_{pump}(LP)$	kW	0.05	0.09	0.08
$\dot{m}_{fluid}(LP)$	kg/s	0.13	0.3	0.3
$\dot{Q}_{exhaust\ HEX}$	kW	70.5	137.5	139.9
$\dot{Q}_{air\ condenser}$	kW	123.6	261.8	262.5
$\dot{m}_{cooling\ air}$	kg/s	6.1	12.9	12.9
$\dot{W}_{additional\ fan}$	kW	0	3.1	3.1
\dot{W}_{system}	kW	15.9	11.7	13.1
η_{system}	%	11.4	4.2	4.7

The frictional losses (Fig. 5c) in the HP expander at the design-point B50 condition increases with the reduction in the vapour quality, due to the increasing two-phase

viscosity (Eq. 25). The increased frictional losses from superheated to the saturated state are linked to the expander exit being in a two-phase state. However, at the C100 extreme off-design condition, from superheated to saturated state, the HP expander frictional losses remain constant, due to the high leakages, that when reunited in node 5 (Fig. 1), increases the vapour quality to near saturated state.

The LP pump flow rate was controlled to maintain an LP expander inlet quality of 0.75, hence, the LP expander efficiency (Fig. 5a) is only marginally influenced by the reduction in the vapour quality of the HP expander. The marginally increasing heat transfer and leakage losses are attributed to a slightly increasing mass flow rate at the LP expander inlet with mixing of streams 2 and 5 (Fig. 3).

Table 5. presents the system level results for the integrated engine cooling and exhaust heat recovery at three points: B50 design-point; C100 off-design point with superheated HP expansion; and optimised C100 off-design point with two-phase HP expansion. Firstly, the combination of a two-phase LP expander and a superheated HP expander at the B50 design-point provided additional 10% of engine crankshaft power (15.9 kW of system net power). Secondly, operating the HP expander under the optimised two-phase state at the C100 extreme off-design point provided a 15% increase in the expander power (12.2 vs. 10.6 kW). Note that, the results presented here reflect the real world constraints for heat recovery systems in transport applications. For example, the condensing temperature range (66-93°C) was typical of that observed in a truck cooling module and the pump efficiencies (55%) were representative of cost-effective components.

4.2. Study 2 - Off-design Operation of the LP Expander

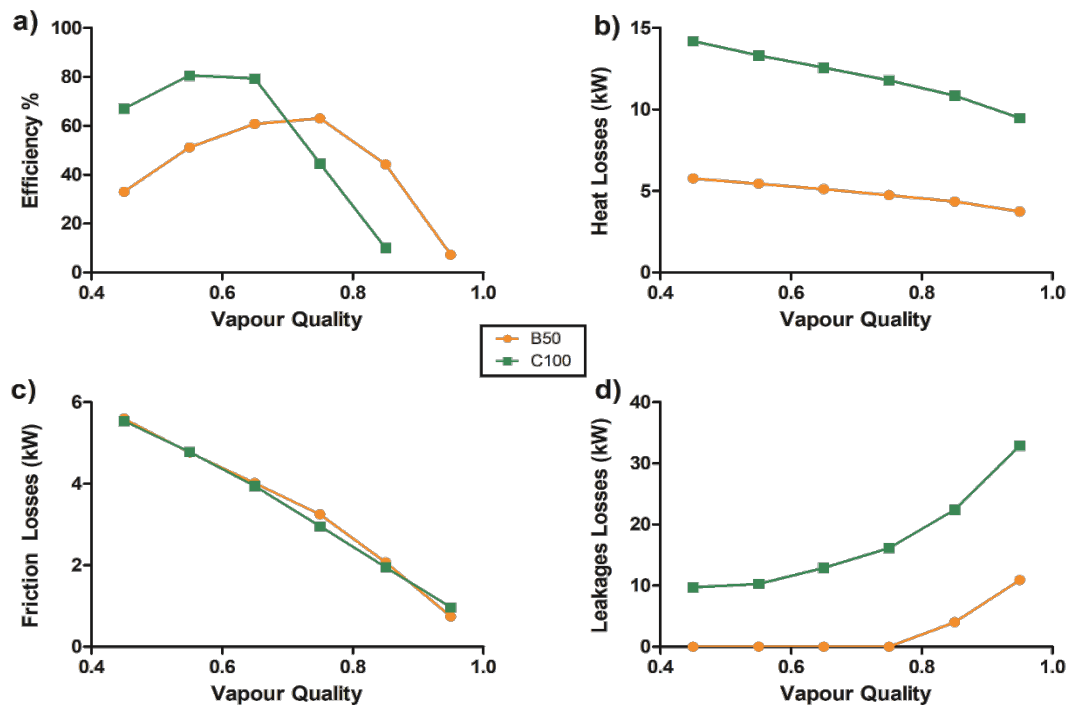


Fig. 6 Study 2: a) expander efficiency, b) heat losses, c) friction losses and d) leakage losses when LP inlet vapour quality was varied, whereas HP inlet fluid flow condition was fixed.

Table 6.

Integrated engine cooling and exhaust heat recovery results at the B50 design-point, C100 extreme off design point with non-optimal and C100 extreme off design point with optimal LP expander inlet vapour quality. All with fixed HP expander fluid flow.

Study 2	Unit	B50	C100	C100
		LP Expander x = 0.75 Design-point	LP Expander x = 0.75, Non-optimal off-design	LP Expander x = 0.55, Optimal off-design
$P_{system\ min}$	bar	0.3	1	1
$T_{system\ min}$	°C	59	89	89
$VFR_{expander(HP)}$		8.6:1	9.6:1	9.6:1
$\dot{W}_{expander(HP)}$	kW	9.1	10.6	10.6
$\dot{W}_{pump(HP)}$	kW	0.3	0.6	0.6
$\dot{m}_{fluid(HP)}$	kg/s	0.047	0.099	0.099
$T_{condensation(LP)}$	°C	67	95	95
$VFR_{expander(LP)}$		4.2:1	1.8:1	1.9:1
$\dot{W}_{expander(LP)}$	kW	7.3	4.9	9.1
$\dot{W}_{pump(LP)}$	kW	0.05	0.09	0.13
$\dot{m}_{fluid(LP)}$	kg/s	0.13	0.3	0.39
$\dot{Q}_{exhaust\ HEX}$	kW	70.5	137.5	137.5
$\dot{Q}_{air\ condenser}$	kW	123.6	261.6	257.6
$\dot{m}_{cooling\ air}$	kg/s	6.1	12.9	12.7
$\dot{W}_{additional\ fan}$	kW	0	3.1	3
\dot{W}_{system}	kW	16	11.7	16
η_{system}	%	11.5	4.2	5.8

The heat transfer losses in the LP expander increase with the reduction in the vapour quality (Fig. 6b), due to the increasing convective heat transfer coefficient. At the B50 design-point condition, nearly 60% of the losses were attributed to heat. At C100 off-design condition, absolute heat transfer losses are more than double than at B50 design condition, due to the higher mass flow rate (increased fluid velocity), and therefore, higher convective heat transfer coefficient.

The frictional losses in the LP expander increases with the reduction in the vapour quality (Fig. 6c), due to the increasing two-phase viscosity (Eq. 25). At the B50 design-point condition, nearly 40% of the losses were attributed to friction. Compared to the HP expander (Fig. 5c), the variation in frictional losses between B50 and C100 conditions for the LP expander were insignificant, firstly, due to a much lower enthalpy drop and viscosity variation across the expander nodes, and secondly, due to the increase in mass flow rate at the C100 condition somewhat being matched by the increased expander rotational speed (1440 vs. 1720 rpm).

Increasing the LP expander inlet vapour quality from the 0.75 value at the B50 design-point introduced leakages (Fig. 6d), due to lower mass flow rate being admitted into the expander as a result of the reducing inlet density. However, at the C100 condition, the LP expander presents an interesting opportunity, where by reducing the vapour fraction to 0.55, a new efficiency peak is observed (Fig. 6a). Here, the increasing heat transfer and frictional losses due to lower vapour quality are negated by the increased power output due to mass flow rate utilisation. Hence, the

LP expander offers significant improvement in expander efficiency (80% vs. 45%) under an inlet vapour fraction of 0.55 at C100 when compared to the reference two-phase inlet state.

Furthermore, for B50 and C100 condition, decreasing the LP expander vapour quality results in lower rate of efficiency drop compared to increasing the vapour quality. Interestingly, this trend matches the behaviour reported in the literature for the case of under/over expansion [24]. Since, higher vapour quality leads to higher specific volume, hence for a fixed BVR, lower outlet pressure and higher enthalpy drop can be achieved.

Table 6 presents the system level results for the integrated engine cooling and exhaust heat recovery at three points: B50 design-point; C100 off-design point with reference two-phase LP expansion; and optimised C100 off-design point with two-phase LP expansion. Operating the LP expander under optimised two-phase state at the C100 extreme off-design point provided an 85% improvement in expander power (9.1 vs. 4.9 kW).

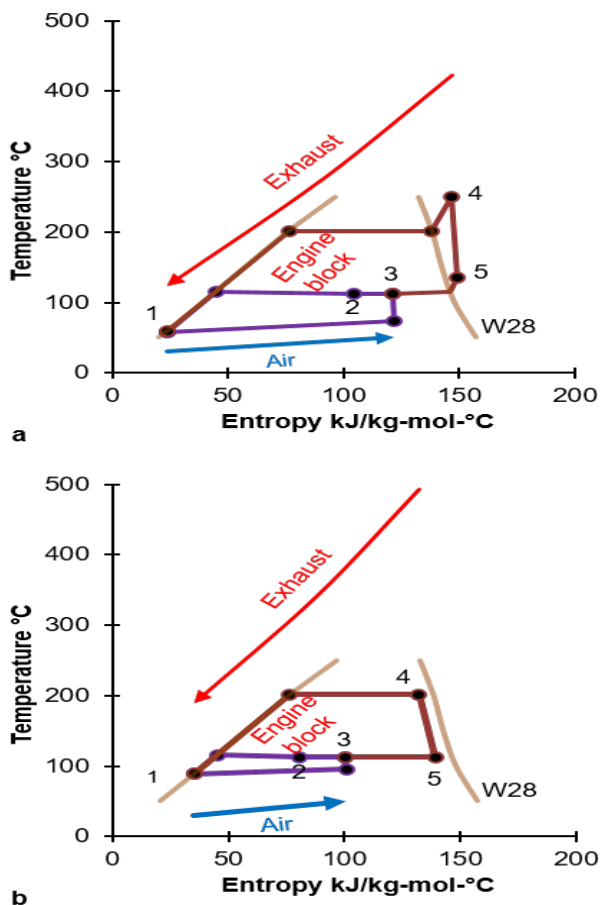


Fig. 7 Temperature-Entropy diagram for the considered next generation of heat recovery system using W28: a) B50 design-point condition in association with two-phase LP expansion and superheated HP expansion, b) C100 extreme off-design optimised condition with two-phase LP and HP expansion.

Fig. 7a presents the T-S diagram for the considered next generation of heat recovery system at the B50 design-point. Recovery of heat, directly from the engine block and the exhaust heat exchanger is performed using W28 as the common working fluid, in association with

two-phase LP expansion and superheated HP expansion. Furthermore, findings from Study 1 and 2 now allow a combined optimisation at the C100 extreme off-design condition. Fig 7b presents the corresponding T-S diagram with LP and HP expansion inlet vapour fraction of 0.55 and 0.9. The combined optimisation of the two-phase operation of the two expanders provided nearly 50% improvement in the system performance (17.4 vs. 11.7 kW of net system power), adding a total of 5.5% to the engine crankshaft power. Note that, the results presented here reflect the real world constraints for heat recovery systems in transport applications. For example, the design pinch point temperature difference (40°C) in the exhaust heat exchanger was representative of low footprint cost-effective components and the fan efficiency (65%) was typical of that observed in a truck cooling module.

In summary, this work introduced the numerical adaptations in the supply valve pressure drop, the heat transfer losses and the frictional losses, which allowed the investigation of two-phase piston expanders for the next generation of integrated engine cooling and exhaust heat recovery system. The rationale for the numerical adaptations were functions of the key thermo-physical fluid properties and published findings from comparable applications. The optimised LP and HP expanders allowed for a combined increase of 5.5% and 10% of engine crankshaft power, during extreme off-design and design point conditions, respectively. When considering the optimised two-phase expander operation without leakages; i.e. design point of the LP expander with $x=0.75$ at B50 in Fig. 6, and the extreme-off design point of the HP expander with $x=0.9$ at C100 in Fig. 5; the friction accounted an average of nearly 25% of the total losses and the heat transfer accounted an average of nearly 20% of the total losses. Due to insufficient experimental results published using two-phase expanders, the scope of future works should include evaluation and reduction in frictional losses by adapting piston air motors as two phase expanders.

5. Conclusions

This work has introduced three numerical adaptations to the semi-empirical expander model, in order to allow investigation of two-phase piston expanders in the next generation of heat recovery systems. The considered expander model accounts for: supply valve pressure drop, heat transfer loss to the expander envelope, leakage mass flow, condensation during expansion and piston frictional losses. The heat recovery system analysed consisted of a low pressure (LP) and a high pressure (HP) expander for integrated engine cooling and exhaust heat recovery using a common water-propanol mixture. Two distinctive engine speed-load conditions were considered, namely, the design point (B50) and the extreme off-design point (C100). Studies were conducted varying the mass flow and the vapour quality for the LP ($x=0.45$ to 0.95) and HP ($x=0.8$ to superheat) expander. The key expander and system level results were:

1. At the design point, the 50°C superheated HP expander with pressure ratio of 10:1 was 86% efficient providing 9.1 kW of power; and the $x=0.75$ two-phase LP expander with a pressure ratio of 4:1 was 62% efficient providing 7.3 kW of power.

2. The HP expander, operated with the preferred two-phase state ($x=0.9$) at the extreme off-design condition provided a 15% improvement in expander power (12.2 vs. 10.6 kW) over the reference inlet state.
3. The LP expander, operated with the preferred vapour quality ($x=0.55$) at the extreme off-design condition provided an 85% improvement in expander power (9.1 vs. 4.9 kW) over the reference inlet state.

Findings 2 and 3 from above demonstrate that improvements in expander power can be achieved by moderating the inlet vapour quality during extreme-off design condition. This was as a result of reduction in the leakage losses due to a density increase following the vapour quality decrease, despite the higher heat transfer and the frictional losses compared to the saturated vapour state.

4. The analysed heat recovery system using the two-phase LP expander and the superheated HP expander provided 15.9 kW with an overall conversion efficiency 11.4%, resulting in 10% additional engine crankshaft power at the design-point.

5. The optimised combined two-phase operation of the expanders at the extreme-off design point improved the system power by nearly 50% (17.4 vs. 11.7 kW), resulting in 5.5% of additional engine crankshaft power.

Finding 5 from above demonstrated that an average of nearly 25% of the total losses were attributed to friction. Therefore, adapting piston air motors as two-phase expanders for experimental evaluation and reduction in frictional losses was a recommended research direction.

Acknowledgments

This work has been conducted under the Advanced Propulsion Centre project EP/R512977/1.

Nomenclature

Abbreviations	
LNG	Liquefied Natural Gas
FMEP	Friction Mean Effective Pressure [bar]
ORC	Organic Rankine Cycle
JT	Joule Thompson
LP	Low Pressure
HP	High Pressure
C100	High-Speed High-Load Condition
B50	Cruise Condition
Variables	
\dot{m}_{in}	Nominal Mass Flow Rate [kg/s]
P_{int}	Net Power [W]
P_{leak}	Leakages Power Loss [W]
x	Vapour quality
ε	Generic Property
ρ	Mass Density [kg/m ³]
$\Delta p_{inlet\ vap}$	Suction Pressure Drop (Vapour Only)
Q	Heat Exchange [W]
A	Heat Loss Area [m ²]
p^*	Reduced Pressure
Pr	Prandtl Number
r_i	Internal Radius [m]
R	Hydraulic Resistance [m/s]
L	Expander Length [m]
V_{sw}	Displacement Volume [m ³]
s	Specific Mass Entropy [J/kg K]
PR	Pressure Ratio
S_f	Engine Speed Factor
\dot{m}_{leak}	Leakages Mass Flow Rate [kg/s]

P_{fric}	Friction Power Loss [W]
p	Pressure [bar]
\dot{m}	Total Mass Flow Rate [kg/s]
h	Specific Mass enthalpy [J/kg]
A_{in}	Inlet Cross Sectional Area [m ²]
$\Delta p_{inlet\ zp}$	Suction Pressure Drop
h_c	Convective Heat Transfer Coefficient [W/m ² K]
α_f	Dittus-Boelter Coefficient
Re	Reynolds Number
k	Thermal Conductivity [W/m K]
p_c	Critical Pressure [bar]
μ	Dynamic Viscosity [Pa s]
N	Engine or Expander Speed [rpm]
BVR	Built-in Volume Ratio
v	Specific Volume [m ³ /kg]
η	Isentropic Efficiency
S	Piston Stroke
Subscripts	
v	Vapour
$2p$	Two-Phase
l	Liquid
is	Isentropic
$dist$	Distributed
0	Node 0
1	Node 1
2	Node 2
3	Node 3
4	Node 4
5	Node 5
6	Node 6

References

- Amsyari, M., Secretary, C., Badak, P. T., Sutedjo, M., Manager, G., Bahana, P. T. I., ... Corporation, E. I. (2007). Using Two-Phase Lng Expanders To Extend Lifetime of Depleting Gas Wells or for Nitrogen Rejection X2. *15th International Conference & Exhibition on Liquefied Natural Gas (LNG 15)*, 55. Barcelona, Spain.
- Automotive Council and Advanced Propulsion Centre. (2018). *The Roadmap Report - Towards 2040: a Guide To Automotive Propulsion Technologies*. Retrieved from <https://www.apcuk.co.uk/app/uploads/2018/06/roadmap-report-26-6-18.pdf>
- Bernagozzi, M., Charmer, S., Georgoulas, A., Malavasi, I., Michè, N., & Marengo, M. (2018). Lumped parameter network simulation of a Loop Heat Pipe for energy management systems in full electric vehicles. *Applied Thermal Engineering*, 141, 617–629. <https://doi.org/10.1016/j.applthermaleng.2018.06.013>
- Bianchi, G., Kennedy, S., Zaher, O., Tassou, S. A., Miller, J., & Jouhara, H. (2017). Two-phase chamber modeling of a twin-screw expander for Trilateral Flash Cycle applications. *Energy Procedia*, 129, 347–354. <https://doi.org/10.1016/j.ijrefrig.2018.02.001>
- BorgWarner. (2018). *Converting Waste Heat into Electrical Energy: BorgWarner's Organic Rankine Cycle*. Auburn Hills.
- Chen, S. K., & Flynn, P. F. (1965). Development of a Single Cylinder Compression Ignition Research Engine. *National Powerplant and Transportation Meetings*. <https://doi.org/https://doi.org/10.4271/650733>
- Derby, M., Lee, H. J., Peles, Y., & Jensen, M. K. (2012). Condensation heat transfer in square, triangular, and semi-circular mini-channels. *International Journal of Heat and Mass Transfer*, 55(1–3), 187–197. <https://doi.org/10.1016/j.ijheatmasstransfer.2011.09.002>
- Dumont, O., Dicke, R., & Lemort, V. (2017). Extrapolability and limitations of a semi-empirical model for the simulation of volumetric expanders. *Energy Procedia*, 129, 315–322. <https://doi.org/10.1016/j.egypro.2017.09.198>

- EU Energy Efficiency Plan. (2011). Brussels.
- Giuffrida, A. (2017). Improving the semi-empirical modelling of a single-screw expander for small organic Rankine cycles. *Applied Energy*, *193*, 356–368. <https://doi.org/10.1016/j.apenergy.2017.02.015>
- Idel'chik, I. E. (1960). Handbook of hydraulic resistance (3rd edition). *Washington*, 517. <https://doi.org/AEC-tr-6630>
- Imran, M., Usman, M., Park, B. S., & Lee, D. H. (2016). Volumetric expanders for low grade heat and waste heat recovery applications. *Renewable and Sustainable Energy Reviews*, *57*, 1090–1109. <https://doi.org/10.1016/j.rser.2015.12.139>
- Kanaś, P., Jedlikowski, A., & Anisimov, S. (2019). The influence of geometrical parameters on heat and mass transfer processes in rotary heat exchangers. *SN Applied Sciences*, *1*(6), 1–16. <https://doi.org/10.1007/s42452-019-0540-2>
- Lemort, V., Declaye, S., & Quoilin, S. (2012). Experimental characterization of a hermeti scroll expander for use in a micro-scale Rankine cycle. *Proceedings of the Institution of Mechanical Engineers, Part A: Journal of Power and Energy*, *226*(1), 126–136. <https://doi.org/10.1177/0957650911413840>
- Lemort, Vincent, Quoilin, S., Cuevas, C., & Lebrun, J. (2009). Testing and modeling a scroll expander integrated into an Organic Rankine Cycle. *Applied Thermal Engineering*, *29*(14–15), 3094–3102. <https://doi.org/10.1016/j.applthermaleng.2009.04.013>
- Oralli, E., Tarique, M. A., Zamfirescu, C., & Dincer, I. (2011). A study on scroll compressor conversion into expander for Rankine cycles. *International Journal of Low-Carbon Technologies*, *6*(3), 200–206. <https://doi.org/10.1093/ijlct/ctr008>
- Panesar, A. S. (2016). An innovative organic Rankine cycle approach for high temperature applications. *Energy*, *115*(March), 1436–1450. <https://doi.org/10.1016/j.energy.2016.05.135>
- Panesar, A. S. (2017). An innovative Organic Rankine Cycle system for integrated cooling and heat recovery. *Applied Energy*, *186*, 396–407. <https://doi.org/10.1016/j.apenergy.2016.03.011>
- Pikra, G., & Rohmah, N. (2019). Comparison of single and double stage regenerative organic Rankine cycle for medium grade heat source through energy and exergy estimation. *International Journal of Renewable Energy Development*, *8*(2), 141–148. <https://doi.org/10.14710/ijred.8.2.141-148>
- Qyyum, M. A., Qadeer, K., Lee, S., & Lee, M. (2018). Innovative propane-nitrogen two-phase expander refrigeration cycle for energy-efficient and low-global warming potential LNG production. *Applied Thermal Engineering*, *139*(April), 157–165. <https://doi.org/10.1016/j.applthermaleng.2018.04.105>
- Saghatoun, S., Zhuge, W., & Zhang, Y. (2014). Review of Expander Selection for Small-Scale Organic Rankine Cycle. *Proceedings of the ASME 2014 4th Joint US-European Fluids Engineering Division Summer Meeting FEDSM2014 August 3-7, 2014, Chicago, Illinois, USA*. <https://doi.org/10.1115/fedsm2014-21904>
- Sánta, R. (2012). The Analysis of Two-Phase Condensation Heat Transfer Models Based on the Comparison of the Boundary Condition. *Acta Polytechnica Hungarica*, *9*(6), 167–180.
- Shah, M. M. (2009). An Improved and Extended General Correlation for Heat Transfer During Condensation. *Hvac&R Research*, *15*(September 2009), 37–41. <https://doi.org/10.1080/10789669.2009.10390871>
- Tchanche, B. F., Lambrinos, G., Frangoudakis, A., & Papadakis, G. (2011). Low-grade heat conversion into power using organic Rankine cycles - A review of various applications. *Renewable and Sustainable Energy Reviews*, *15*(8), 3963–3979. <https://doi.org/10.1016/j.rser.2011.07.024>
- Vasuthevan, H., & Brümmer, A. (2016). Thermodynamic Modeling of Screw Expander in a Trilateral Flash Cycle. *23rd International Compressor Engineering Conference*.



© 2019. This article is an open access article distributed under the terms and conditions of the Creative Commons Attribution (CC BY) license (<http://creativecommons.org/licenses/by/4.0/>).